THE JOURNAL OF PHYSICAL CHEMISTRY B

Article

pubs.acs.org/JPCB

Proton Diffusion in the Hexafluorophosphoric Acid Clathrate Hydrate

Laura Bedouret,[†,‡] Patrick Judeinstein,[§,∥,⊥] Jacques Ollivier,[‡] Jérôme Combet,[‡,#] and Arnaud Desmedt*[,†]

[†]Groupe de Spectroscopie Moléculaire, ISM UMR5255 CNRS - Université de Bordeaux, 351 cours de la Libération, F-33405 Talence, France

[‡]Institut Laue Langevin, 6 rue Jules Horowitz, B.P. 156, 38042 Grenoble Cedex 9, France

[§]Institut de Chimie Moléculaire et des Matériaux d'Orsay, UMR 8182 CNRS, Université Paris Sud, Bât. 410, F-91405 Orsay Cedex, France

[∥]Laboratoire de Physique des Solides, UMR 8502 CNRS, Université Paris Sud, Bât. 510, F-91405 Orsay Cedex, France

[⊥]Laboratoire Léon Brillouin, UMR12 CEA-CNRS, CEA Saclay, F-91191 Gif sur Yvette Cedex, France

ABSTRACT: The hexafluorophosphoric acid clathrate hydrate is known as a "super-protonic" conductor: its proton conductivity is of the order of 0.1 S/cm at ca. room temperature. The long-range proton diffusion and the associated mechanism have been analyzed with the help of incoherent quasi-elastic neutron scattering (QENS) and proton pulsed-field-gradient nuclear magnetic resonance (^{1}H PFG-NMR). The system crystallizes into the so-called type I clathrate structure (SI) at low temperature and into the type VII structure (SVII) above ca. 230 K with a melting point close to room temperature. While, in the SI phase, no long-range proton diffusion is observed (at least faster than the present measurement capabilities, i.e., 10^{-7} cm^2·s^{-1}) with respect to the probed time scale, both techniques evidence a long-range proton diffusion process in the SVII phase (3.85×10^{-6} cm^2·s^{-1} at 275 K with an activation energy of 0.19 ± 0.04 eV). QENS experiments lead to modeling the microscopic mechanism of the long-range proton diffusion by means of a Chudley−Elliot jump diffusion model with a characteristic jump distance of 2.79 ± 0.17 Å. In other words, the long-range diffusion occurs through a Grotthus mechanism with proton jumping from one water-oxygen site to another. Moreover, the analysis of the proton diffusion for hydration numbers greater than 6 (i.e., in the SVII structure) reveals that the additional water molecules coexisting with the SVII structure act as a "structural defect" barrier for the proton diffusivity, responsible for the conductivity.

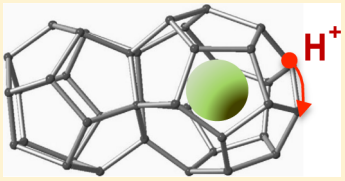

1. INTRODUCTION

Clathrate hydrates are crystals formed by means of a framework of H-bonded water molecules containing inclusion cavities within which guest molecules are located.[1,2] The natural abundance of this composite as well as its peculiar structure and composition variability, which lead to various specific physical−chemical properties,[3] have given birth to a huge interest from the scientific community.[4,5] Ionic clathrate hydrates constitute one interesting class of these materials. The confinement of ionic guest molecules within a water substructure containing the appropriate counterions leads to clathrate hydrates possessing specific add-ons in terms of applicative issues like gas separation, gas storage, or solid electrolyte.[6] Moreover, the specific ionic interaction generated by the inclusion of ionic species confers to these systems peculiar physicochemical properties such as high proton conductivity in the case of acidic clathrate hydrates.

Several research groups have focused on the structural and electrochemical properties of proton conducting clathrate hydrates made with alkyl ammonium hydroxide[7−10] or strong monoacids.[11−13] Among these ionic clathrate hydrates, the hexafluorophosphoric acid (HPF_6) clathrate hydrates have melting points close to room temperature and exhibit high conductivities typical of superionic conductors (of the order of 10^{-1} S·cm^{-1} at room temperature).[13] Depending on the hydration number (typically varying between 4 and 7.67 H_2O molecules per HPF_6 acidic molecule), the HPF_6 clathrate hydrates crystallize either in the so-called type I structure (denoted SI)[12] or in the type VII structure (denoted SVII).[14] Moreover, a structural phase transition between SI and SVII structures is observed at ca. 230 K for hydration numbers greater than 6. In both structures, the acid is deprotonated, leading to cationic cages filled with anions. The SI structure possesses two types of cages (small 5^{12} cages and large $5^{12}6^2$ cages) in which only the large cages are filled with the anionic guests (leading to an ideal formula of HPF_6·7.67H_2O), while the SVII structure is made of a single type of cages ($4^6 6^8$), all filled with guests (leading to an ideal formula of HPF_6·6H_2O). In both phases, the excess proton existing in the water substructure leads to the violation of the so-called ice rule (i.e., each water molecule accepts and donates two hydrogen bonds), so that the excess proton exhibits a high mobility at the origin of the high conductivity. Interestingly, the best conductivity is obtained for hydration number equal to 6, i.e., in the SVII structure; such a behavior has been interpreted in terms of favorable proton pathways with respect to the SI structure.[13] However, within the SVII structure phase, increasing the

Special Issue: Physics and Chemistry of Ice 2014

Received: April 28, 2014
Revised: June 18, 2014

   dx.doi.org/10.1021/jp504128m | J. Phys. Chem. B XXXX, XXX, XXX−XXX

hydration number leads to a decrease in the proton conductivity. The proton pathways hypothesis thus presupposes that increasing the hydration number leads to a decrease in the number of favorable proton pathways in the SVII structure. Such a feature should directly have an impact on the diffusivity of proton in the SVII clathrate hydrates. In order to shed more light on this issue, the aim of the present paper is to investigate the long-range proton diffusion in the hexafluorophosphoric SVII clathrate hydrate with the help of incoherent quasi-elastic neutron scattering (QENS) and proton pulsed-field-gradient nuclear magnetic resonance (^{1}H PFG-NMR). Both techniques are particularly appropriate for such a problem, since they allow one to access the proton displacements on a complementary time and space scale, i.e., at a microscopic scale with ^{1}H PFG-NMR and at atomic level with QENS experiments. Indeed, proton displacements greater than 100 nm over the millisecond time scale can be probed with the help of the ^{1}H PFG-NMR technique and incoherent quasi-elastic neutron scattering techniques yield only proton dynamics (the hydrogen atom possesses the largest existing incoherent scattering cross section, making the contribution of all other atoms negligible) to be investigated on time scales typically ranging from the nanosecond to the picosecond over a characteristic distance ranging from 0.1 up to 1 nm. Through the investigation of proton motions across such a wide range of characteristic time and spatial scales, the combination of these two techniques is a powerful strategy for providing experimental insights into the proton transport mechanism within ice-like systems that ionic clathrate hydrates represent.

2. EXPERIMENTAL DETAILS

The HPF_6 solution was obtained by diluting a 60 wt % HPF_6 commercially available solution with distilled water under an inert atmosphere. Two solutions, $HPF_6{\cdot}7.67H_2O$ and $HPF_6{\cdot}6.5H_2O$, have been analyzed by means of ^{1}H PFG-NMR experiments, carried out on a 9.4 T Bruker Avance 400 NMR spectrometer equipped with a Bruker 5 mm broadband probe with a z-axis gradient. Temperatures were controlled within the 200−300 K range with a Bruker BVT3000 system (±0.5 K regulation). Temperature calibration was performed before each set of measurements by using the standard procedure with a reference methanol sample. Liquid samples were introduced in poly tetrafluoroethylene (denoted PTFE) tubes placed in classic NMR tubes, and were crystallized in the cryostat. NMR measurements have been performed in heating and cooling cycles at selected temperatures between room temperature and 190 K (with a temperature equilibration time of 30 min). The NMR resonance frequency was 400.13 MHz, and the $\pi/2$ pulse length was calibrated to 11 μs. Self-diffusion coefficient measurements were performed by using a method based on a combination of pulsed field gradient stimulated echo (PFGSE) and longitudinal eddy-current delay (LED) sequences using two spoil gradients.[15]

The relative echo amplitude E is attenuated due to translational diffusion, which is related to the self-diffusion coefficient D by[16]

$$E(q, \Delta) = \exp\left(-D{\cdot}q^2{\cdot}\left(\Delta - \frac{\delta}{3}\right)\right) \quad \text{with } q = \gamma{\cdot}\delta{\cdot}g \tag{1}$$

where g and δ are the magnitude and duration of the two gradient pulses, Δ is the time interval between these pulses, and γ is the gyromagnetic ratio of the nucleus under study. Experimentally, E is the ratio of signal areas obtained with and without gradient pulses. The magnitude of the pulsed field gradient was varied as $0 \le g \le 45$ G cm^{-1}; the diffusion time Δ between two pulses was fixed at 100 ms, and the gradient pulse duration, δ, was set between 2 and 22 ms, depending on the diffusion coefficient of the mobile species.

Quasi-elastic neutron scattering (QENS) experiments were carried out at the Institut Laue Langevin (Grenoble, France). The $HPF_6{\cdot}7.67H_2O$ solution was introduced between two PTFE foils (10 μm thickness, Goodfellow) in an indium-sealed aluminum flat sample holder in order to avoid the problems of corrosion. Due to the high incoherent cross section of the hydrogen atoms, we can reasonably consider that they entirely dominate the scattered incoherent intensity. The sample thickness was less than 0.2 mm, so that the transmission was greater than 90% and the multiple scattering effects were negligible. The angle between the incident beam and the plane of the sample holder was 135°. High-resolution (HR-QENS) spectra were recorded on the backscattering spectrometer IN16@ILL[17] using the Si(111) monochromator and analyzers (λ_o = 6.27 Å with an energy resolution of $\Delta E \approx 1$ μeV). Given the scattering angles covered by the analyzers, the momentum transfers ($\hbar Q$) probed correspond to Q values in the range 0.2−1.9 Å^{-1}. The first part of the HR-QENS experiment has been the acquisition of an elastic fixed window scan (denoted EFWS), which consists of measuring the purely elastic scattering as a function of temperature. For this measurement, after crystallization of the acidic solution, the sample has been heated from 85 to 310 K and then cooled from 300 to 2 K (the acquisition time was 150 s per step with a heating/cooling rate of 0.4 K/min). HR-QENS spectra (±15 μeV) were then recorded (data collection time of ca. 9 h) at 2 K (providing access to the instrumental resolution function) and 230 K for subsequent spectral analysis. In order to probe dynamical processes occurring on a shorter time scale, QENS experiments were also performed using the time-of-flight (ToF) spectrometer IN5@ILL[18] for which the scattering angles (2θ) ranged from 5 to 135°. Two energy resolutions of $\Delta E \approx 100$ μeV (λ_o = 5 Å) and $\Delta E \approx 15$ μeV (λ_o = 10 Å) were used, with an acquisition time of 3 and 6 h, respectively. Spectra were recorded at 50 K (used as an instrumental resolution function), 230, 255, and 280 K in order of increasing temperature.

The raw data were corrected for detector efficiency and sample-geometry dependent attenuation, and the background was subtracted using the measurement for an empty sample container (including the PTFE foils and the indium sealing). Detectors containing Bragg peak intensity were carefully checked and removed from the analysis. Several detectors were grouped together in order to improve the statistics. All of these procedures were carried out at the ILL using standard software.[19] Data analysis has been carried out using the program NEMO.[20]

The reduced QENS spectra recorded as a function of scattering vector, Q, and energy transfer, $\hbar\omega$, are related to the scattering law, $S(Q, \omega)$, by[21]

$$S_{exp}(Q, \omega) = F(Q)e^{-\hbar\omega/k_BT}S(Q, \omega) \otimes R(Q, \omega) + B(Q, \omega) \tag{2}$$

where $F(Q)$ is the scaling factor for which the Q dependence is due to the Debye−Waller factor [$\exp(-Q^2\langle u^2\rangle)$, where $\langle u^2\rangle$ is the mean square displacement], T is the temperature, and k_B is the Boltzmann constant. $B(Q, \omega)$ is the background term

dx.doi.org/10.1021/jp504128m | J. Phys. Chem. B XXXX, XXX, XXX−XXX

reproducing the inelastic contributions in the quasi-elastic region. The function $R(Q, \omega)$ represents the experimental energy resolution that acts as a time-filter on the scattering law. Indeed, the width of the energy resolution function (noted ΔE hereafter) gives the limit of the time scale on which a given motion will be observed on the experimental spectra: it allows the definition of an observation time ranging from nanoseconds (HR-QENS) to picoseconds (ToF-QENS).

3. RESULTS

3.1. Phase Transition Sequences. The EFWS intensities averaged over all scattering angles are shown in Figure 1 for the heating and cooling cycles of the $HPF_6 \cdot 7.67H_2O$ sample. In the liquid phase (denoted LP in Figure 1), the negligible observed elastic intensities are due to the fast Brownian molecular motions of the molecules and more especially to the long-range molecular diffusion at the origin of the broadening of the whole QENS spectra. The melting point is observed at ca. 295 K in agreement with conductivity measurements,[11] X-ray diffraction analysis,[12,14,22] and differential scanning calorimetry (DSC) measurements.[13] The liquid−solid transition is characterized by a hysteresis in the EFWS intensities as expected for such a first-order transition. At the freezing point observed at ca. 282 K, the abrupt increase of the elastic intensities is due to the "freezing" of the long-range translational motions of molecular species. The acidic solution crystallizes in the type VII clathrate structure (space group $Im3m$ with $a \approx 7.7$ Å) as determined by means of X-ray diffraction.[13] Between ca. 180 K and ca. 225 K, there is a change in the slope of the EFWS intensities curve with a clear difference between the heating cycle and the cooling cycle. This dynamical transition observed in the EFWS intensities may then be related to the structural transition from a high temperature SVII structure to the low temperature SI clathrate structure. Indeed, the powder X-ray diffractogram recorded at 111[12] and 93 K[13] indicated that the $HPF_6 \cdot 7.67H_2O$ clathrate hydrate adopts a type I structure (space group $Pm\bar{3}n$ with $a \approx 11.7$ Å) in this temperature range. The SI−SVII transition possesses a strong reconstructive character, despite the group to subgroup relationship existing between these two crystalline phases. The SI unit cell comprises 46 water molecules forming two types of cages (two small 5^{12} cages and six large $5^{12}6^2$ cages) with only the large cages filled with the PF_6^- anions, so that the ideal stoichiometry of the SI structure corresponds to the one of the present sample. The SVII unit cell contains 24 water molecules forming one single $4^6 6^8$ type of cages, all occupied by PF_6^- ions, leading to a ratio of 6 water molecules per HPF_6 molecule.[14] The present sample, $HPF_6 \cdot 7.67H_2O$, although an ideal stoichiometry for the SI structure, exhibits consequently an excess of water molecules when forming the SVII structure. This additional water phase (corresponding to ca. 22% of the water molecules) may be at the origin of ice Bragg peaks observed by means of X-ray diffraction and thermal anomalies observed at about 273 K (corresponding to the water melting point) on DSC curves.[13] The SI−SVII transition then implies the structural transformation of a single phase (SI) to two crystal phases (SVII and ice) by including or excluding water molecules from the clathrate phase. Such a first order reconstructive transition involves a broad thermal anomaly, as observed on the DSC curve in a similar temperature region with a maximum of the endothermic peak at ca. 230 K.[13] Moreover, this structural transition involves freezing of proton dynamical processes and is related to the fact that the SVII clathrate structure is a better proton conductor than the SI clathrate structure.[13] Thus, in the SI phase, all proton motions appear frozen on the probed time scale, and the slight increase of the elastic intensity is due to the decreasing amplitudes of external and internal vibrations of the molecules (associated with the Debye−Waller factor). Subsequently, the neutron scattering data investigations will focus in the SVII phase between 230 and 280 K, i.e., on the proton dynamics in the $HPF_6 \cdot 7.67H_2O$ sample.

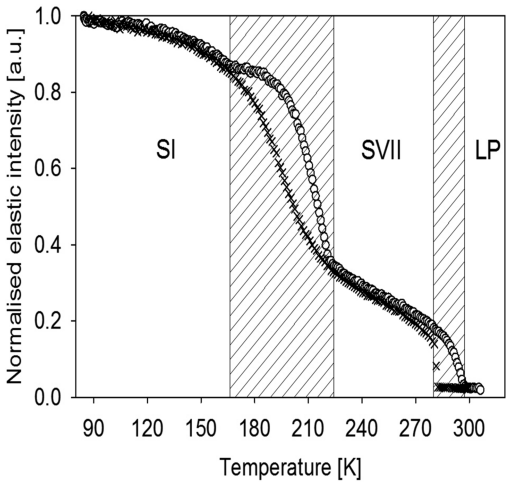

Figure 1. Fixed window scan average over all scattering angles and recorded by cooling (crosses) and by heating (open circles) a $HPF_6 \cdot 7.67H_2O$ clathrate hydrate sample. LP, SI, and SVII denote the liquid and the type I and type VII clathrate phases, respectively.

3.2. ^{1}H NMR. Representative echo attenuations performed on the $HPF_6 \cdot 7.67H_2O$ sample at different temperatures are shown in Figure 2. In contrast with the single diffusive mode observed at 305 K in the liquid phase, the measured PFG-NMR signal appears to be nonlinear (on a logarithmic scale) in the solid phase. This could originate from either a confined diffusive process or a bimodal diffusive process. In order to preclude any diffusion process by using specific molecular transport models, inverse Laplace transform (ILT) calculations of the experimental echo attenuation data have been recently

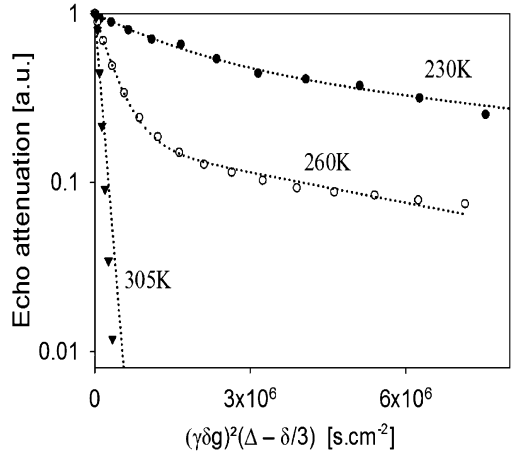

Figure 2. ^{1}H PFG-NMR spin echo attenuation for the $HPF_6 \cdot 7.67H_2O$ clathrate hydrate at selected temperatures (recorded by heating the sample). Continuous lines represent fits of the experimental data by means of eq 3 (see text for details).

dx.doi.org/10.1021/jp504128m | J. Phys. Chem. B XXXX, XXX, XXX−XXX

performed.[23] For our results, these calculations showed that a bimodal motion process has to be used, as a reliable approximation. The spin echo attenuation has then been fitted by means of the following expression:

$$E(q, \Delta) = p \exp\left(-D_a q^2\left(\Delta - \frac{\delta}{3}\right)\right) + (1 - p) \exp\left(-D_b q^2\left(\Delta - \frac{\delta}{3}\right)\right) \quad (3)$$

which gives access to the macroscopic diffusion coefficients D_a and D_b of the two types of proton populations of fractions p and $(1 - p)$. In the SVII phase, the spin echo attenuations have been well reproduced by considering eq 3, as shown in Figure 2. Over the probed temperature range, it has been measured that a fraction $p = 0.17 \pm 0.03$ of the protons are characterized by diffusion coefficients, D_a, exhibiting no significant temperature dependence. The average diffusion coefficient of this dynamical process is $(1.2 \pm 0.5) \times 10^{-8}$ cm^2/s, which is below the detection limit of the NMR spectrometer. Moreover, these values are independent of the experimental conditions (i.e., the duration of the gradient pulse δ, the diffusion delay Δ, and the sample preparation): it follows that this diffusion mode cannot be attributed to any confinement effect, as already mentioned. It is attributed to proton diffusion occurring in the excess phase of the water molecules mixed in the SVII phase of the $HPF_6 \cdot 7.67H_2O$ clathrate hydrate: the fitted fraction ($p = 0.17 \pm 0.03$) of protons, immobile with respect to the NMR probed time scale, is in agreement with the 22% water molecules not participating in the SVII structure in the $HPF_6 \cdot 7.67H_2O$ sample. In order to confirm this hypothesis, the spin echo attenuations recorded on the $HPF_6 \cdot 6.5H_2O$ have been fitted with expression 3; a fraction $p = 0.08 \pm 0.03$ of the proton has been determined with diffusion coefficients D_a at the detection limit of the NMR spectrometer. Such a fraction is again in agreement with the water molecules excess expected in the $HPF_6 \cdot 6.5H_2O$ sample (i.e., 7.7% of the water molecules). The major contribution of the echo attenuation (due to proton fractions of $(1 - p) = 0.83 \pm 0.03$ and $(1 - p) = 0.92 \pm 0.03$ in the samples $HPF_6 \cdot 7.67H_2O$ and $HPF_6 \cdot 6.5H_2O$, respectively) is characterized by diffusion coefficients D_b represented in Figure 3. For both samples, the diffusion coefficients have similar values. In other words, the diffusion is characteristic of the same structural phase: this is thus a signature of long-range proton diffusion in the SVII clathrate hydrate structure.

The temperature evolution of the diffusion coefficient measured by means of ^{1}H PFG-NMR is in agreement with the neutron scattering EFWS, previously discussed. Indeed, our measurements show that the liquid to solid transition is characterized by an abrupt drop of the diffusion coefficient (from $(3.8 \pm 0.2) \times 10^{-5}$ cm$^2 \cdot$s^{-1} at 296 K to $(3.85 \pm 0.16) \times 10^{-6}$ cm$^2 \cdot$s^{-1} at 275 K in the case of the $HPF_6 \cdot 6.5H_2O$ sample). At 230 K, the diffusion coefficient reaches a value of $(6.05 \pm 1.05) \times 10^{-7}$ cm$^2 \cdot$s^{-1}; in the SI clathrate phase (i.e., below ca. 225 K), the long-range proton diffusion occurs on a time scale not accessible with the NMR spectrometer, i.e., the associated diffusion coefficient is lower than ca. 10^{-7} cm^2/s. Finally, as observed in the analysis of the neutron scattering EFWS, a hysteresis of the diffusion coefficients is observed at the SI–SVII structural phase transition.

3.3. QENS. QENS spectra (averaged over all the scattering angles) recorded on the $HPF_6 \cdot 7.67H_2O$ clathrate hydrate at 230 K in the SVII phase are shown in Figure 4. With respect to the HR-QENS energy resolution (i.e., $\Delta E \approx 1$ μeV), one can observe a broadening of the HR-QENS spectra, together with a small elastic contribution. This observation is in agreement with the ^{1}H PFG-NMR results, indicating the coexistence of long-range proton transport in the SVII phase and immobile "ice" protons (with respect to the probed time scale). Moreover, the ToF-QENS spectrum recorded with the 100 μeV energy resolution exhibits a large elastic component together with a quasi-elastic component significantly broader than the ones observed with the HR-QENS spectra. These observations suggest the existence of dynamical processes occurring on a time scale significantly shorter than the one characteristic of the HR-QENS data. Such hierarchical dynamics processes are expected in an ionic clathrate hydrate: the long-range translational diffusion of proton results from various localized molecular motions such as molecular species reorientations.[24,25] Considering that these two types of dynamical processes are not coupled, the classical incoherent neutron scattering law of an ionic clathrate hydrate is given by

$$S_{\text{clathrate}}(Q, \omega) = S_{\text{TD}}(Q, \omega) \otimes S_{\text{LD}}(Q, \omega) \quad (4)$$

where $S_{\text{TD}}(Q, \omega)$ and $S_{\text{LD}}(Q, \omega)$ are the incoherent neutron scattering laws due to the long-range proton diffusion and to the localized diffusive motions, respectively (in the following, "TD" refers to translational diffusion and "LD" refers to localized diffusion). The long-range diffusive motion component $S_{\text{TD}}(Q, \omega)$ can be represented by a single Lorentzian function, $L(\Delta_{\text{TD}})$,[21]

$$L(\Delta_{\text{TD}}) = \frac{1}{\pi} \frac{\Delta_{\text{TD}}(Q)}{\Delta_{\text{TD}}(Q)^2 + \omega^2} \quad (5)$$

for which $\Delta_{\text{TD}}(Q)$ is the half width at half-maximum (denoted HWHM). Moreover, since a proton performing localized motions visits a finite spatial volume, the $S_{\text{LD}}(Q, \omega)$ contribution is the sum of an elastic term and a Lorentzian function $L(\Delta_{\text{LD}})$ of HWHM Δ_{LD}:[25]

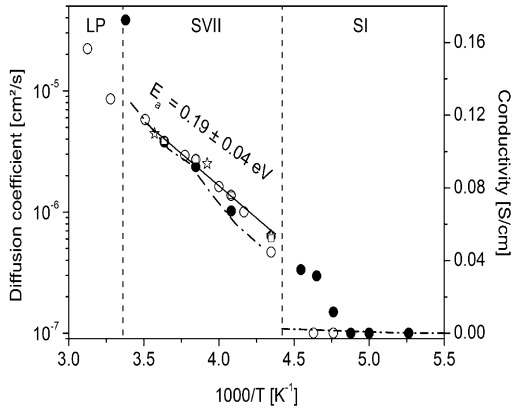

Figure 3. Arrhenius plots of the diffusion coefficients of the $HPF_6 \cdot 6.5H_2O$ clathrate hydrate (open circles, heating cycle; filled circles, cooling cycle) measured by means of PFG-NMR experiments and of the $HPF_6 \cdot 7.67H_2O$ clathrate hydrate measured by means of PFG-NMR (open squares) and QENS (stars) experiments. The activation energy E_a determined with all sets of measurements in the SVII phase is reported on the figure (fitted Arrhenius law shown as a continuous line). In the SI phase, all values correspond to the detection limit of the NMR spectrometer (no significant spin echo attenuation is observed at these temperatures, and the value is set to 10^{-7} cm^2/s). The dash-dotted line is the conductivity adapted from ref 11 for phase SI and from ref 13 for phase SVII.

dx.doi.org/10.1021/jp504128m | J. Phys. Chem. B XXXX, XXX, XXX–XXX

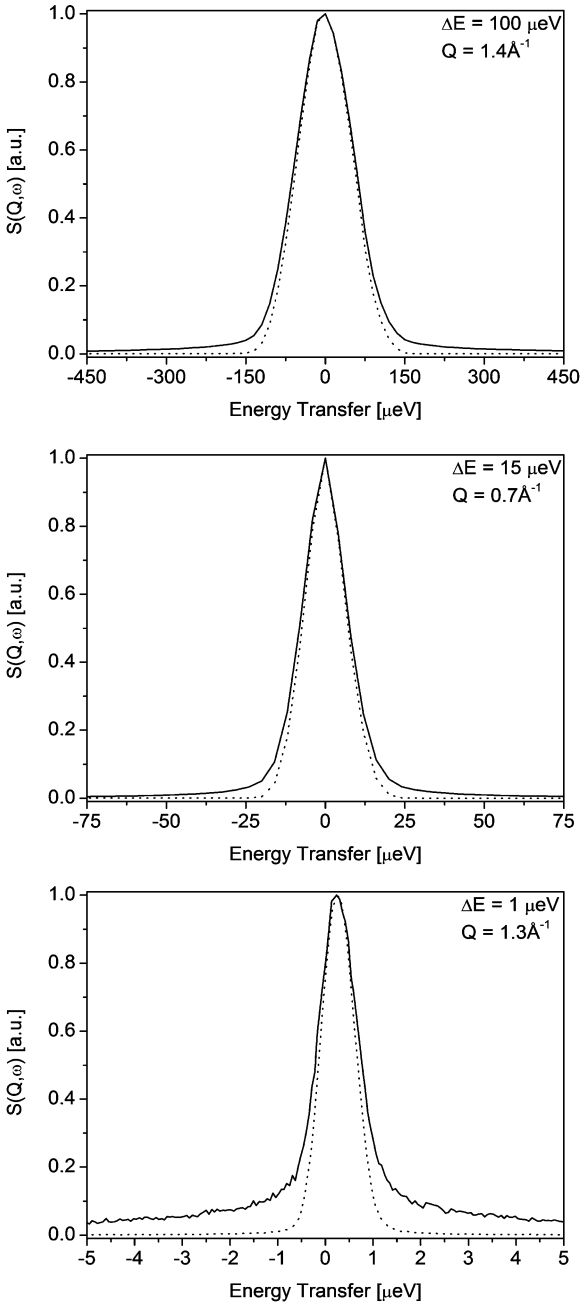

Figure 4. Comparison between the resolution function (dotted lines) and QENS spectra recorded at 230 K (continuous lines) averaged over all the scattering angles and with the energy resolution indicated on the figure.

$$S_{LD}(Q, \omega) = A_0(Q)\delta\omega + [1 - A_0(Q)]L(\Delta_{LD}) \quad (6)$$

Thus, adopting a phenomenological approach, the scattering law (eq 4) of an ionic clathrate hydrate writes as the sum of two Lorentzian functions:

$$S_{clathrate}(Q, \omega) = A_0(Q)L(\Delta_{TD}(Q)) + [1 - A_0(Q)]L(\Delta_{TD}(Q) + \Delta_{LD}) \quad (7)$$

where $A_0(Q)$ is the elastic incoherent structure factor (noted EISF hereafter) which corresponds to the elastic component associated with the localized diffusive motions and $\Delta_{TD}(Q)$ and Δ_{LD} are the half width at half-maxima (HWHMs) of the Lorentzian functions reproducing the quasi-elastic broadenings respectively due to the long-range proton diffusion and to localized motions. Finally, as mentioned in the analysis of ^{1}H PFG-NMR data, the $HPF_6 \cdot 7.67H_2O$ sample is constituted of the type VII clathrate hydrate and of excess water, most probably forming an ice phase as previously mentioned, so that the scattering law of the studied sample writes as

$$S(Q, \omega) = \sigma S_{clathrate}(Q, \omega) + (1 - \sigma)S_{ice}(Q, \omega) \quad (8)$$

where σ represents the fraction of protons participating to the clathrate phase (assuming that 22% of the water molecules participate in the ice phase, one obtains $\sigma = 0.8$) and $S_{ice}(Q, \omega)$ is the incoherent scattering law due to ice. According to previous QENS analysis of clathrate hydrate systems,[26] the ice scattering law gives rise to elastic-like scattering with respect to the probed time scale and then reduces to a Dirac function. Thus, the combination of eqs 7 and 8 leads to the following scattering law:

$$S(Q, \omega) = (1 - \sigma)\delta(\omega) + \sigma\{A_0(Q)L(\Delta_{TD}) + [1 - A_0(Q)]L(\Delta_{TD} + \Delta_{LD})\} \quad (9)$$

The whole set of data (i.e., the QENS spectra recorded at the three studied temperatures as a function of the momentum transfer, the energy transfer, and the energy resolution) has been fitted with the help of the phenomenological eq 9. All the scattering angles have been fitted independently, and the free parameters were the scaling amplitude $F(Q)$, the flat background $B(Q)$, and relevant parameters characterizing the proton dynamics, i.e., the structure factor $A_0(Q)$ and the broadening width $\Delta_{TD}(Q)$ and Δ_{LD}. In the fitting procedure, it was difficult to unambiguously determine a single value of the QENS broadening, Δ_{LD}. As previously mentioned,[24,25] this is due to the fact that such localized diffusive motions give rise to several QENS components. In the present work, these QENS components are reduced to a single phenomenological one, as described in eq 9. Limitation to $\pm 10\Delta E$ of the energy window used to fit the data leads to measurement of an average Δ_{LD} value (which did not significantly depend on the momentum transfer whatever the energy resolution) of 45 ± 15, 260 ± 140, and 618 ± 280 μeV at 230, 255, and 280 K, respectively. This localized dynamical process corresponds to mean characteristic times, given in Table 1, associated with an activation energy of 0.24 ± 0.04 eV. Unfortunately, the truncation of the energy windows prevails from the determination of meaningful structure factors. Nevertheless, this methodological approach yields a good agreement between the experimental points and the phenomenological scattering law (Figure 5) and allows the measurement of an accurate HWHM due to long-range proton diffusion, $\Delta_{TD}(Q)$, of interest in the present study. As shown in Figure 6, the study of the long-range diffusion is possible when the corresponding HWHM matches the energy resolution: the

Table 1. Characteristic Times Associated with the Long-Range Translational Diffusion, $\langle\tau_{TD}\rangle$, and with the Localized Diffusive Motions, $\langle\tau_{LD}\rangle$, in the Hexafluorophosphoric Acid Clathrate Hydrate (See Text for Details)

T (K)	$\langle\tau_{LD}\rangle$ (ps)	$\langle\tau_{LD}\rangle$ (ps)
280	30.1 ± 1.9	1.1 ± 0.5
255	51.6 ± 2.2	2.5 ± 1.2
230	203.0 ± 12	14.4 ± 4.8

dx.doi.org/10.1021/jp504128m | J. Phys. Chem. B XXXX, XXX, XXX−XXX

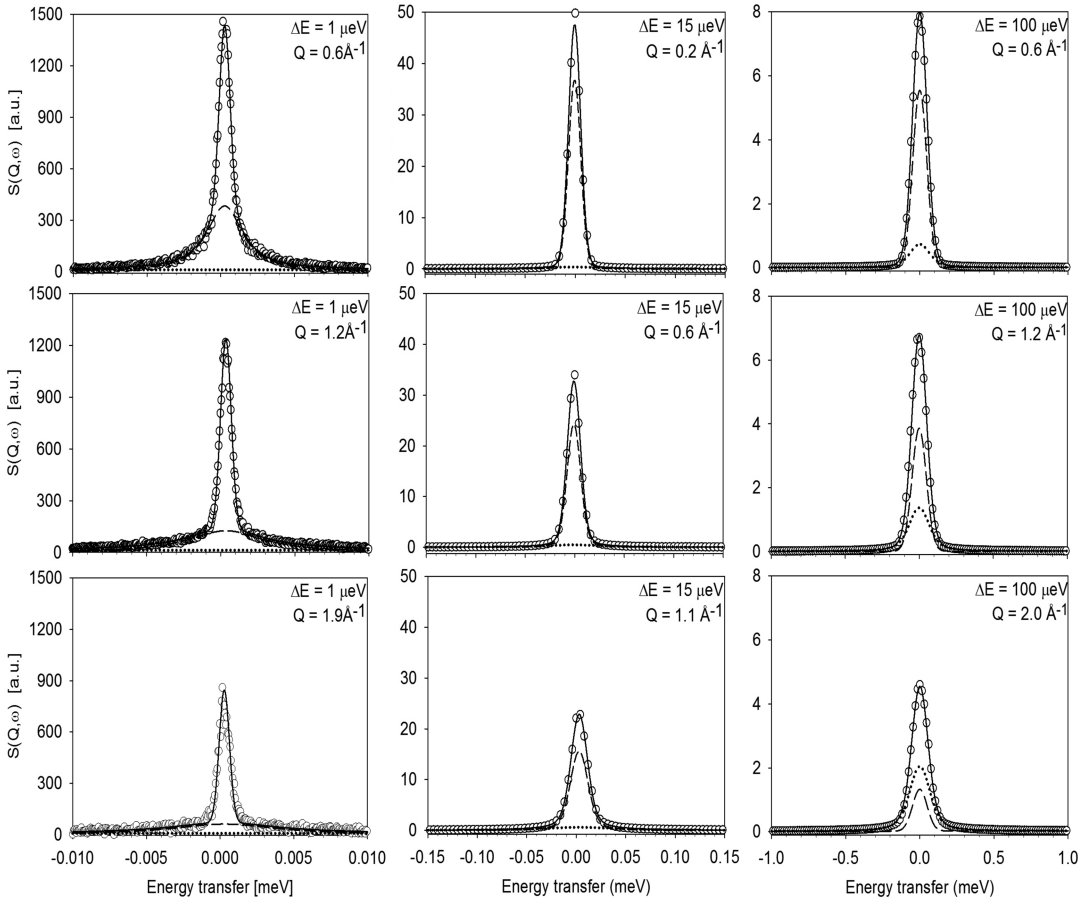

Figure 5. Comparison between the experimental QENS spectra (circles) and the fitted scattering law (continuous lines) of the $HPF_6{\cdot}7.67H_2O$ sample recorded at 230 K for various energy resolution and momentum transfer values indicated in the figure. The Lorentzian functions corresponding to long-range translational diffusion (dashed lines) and localized diffusive motions (dotted lines) are shown in each spectrum.

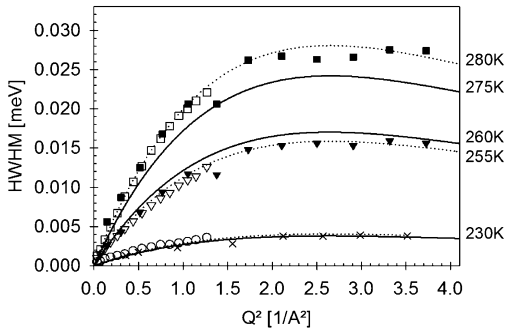

Figure 6. Momentum transfer dependence of the translational HWHM measured by means of QENS experiments at 280 K (squares), 255 K (triangles), and 230 K (circles) [open symbols: IN5, λ_0 = 10 Å, $\Delta E \approx 15$ μeV; filled squares and triangles: IN5, λ_0 = 5 Å, $\Delta E \approx 100$ μeV; crosses: IN16, λ_0 = 6.27 Å, $\Delta E \approx 1$ μeV]. The continuous lines represented the HWHMs calculated according to the Chudley–Elliot model (see text for details) with the help of the diffusion coefficients measured by means of ^{1}H PFG-NMR experiments (at temperatures indicated on the figure), and the dotted lines are the fit result of such a model to the QENS data.

values of $\Delta_{TD}(Q)$ are determined at all studied temperatures for the 15 μeV resolution in the small Q region. In the large Q region, the translational broadening is resolved with the 100 μeV resolution at 280 and 255 K, while it becomes too narrow at 230 K to be disentangled from the energy resolution function of the time-of-flight spectrometer. At this temperature, the QENS spectra obtained with the 1 μeV resolution of the backscattering spectrometer are necessary to retrieve the translational broadening.

On the basis of Fick's law, the HWHMs of the translational QENS component vary according to $D_{TD}Q^2$, where D_{TD} is the self-diffusion coefficient of the protons.[21] At large Q values, the Q^2 dependence of the experimental $\Delta_{TD}(Q)$ values clearly deviates from a simple linear law (see Figure 6). Such a behavior can be reasonably associated in this case to a microscopic mechanism of proton diffusion occurring through jumps between sites. In this crystalline material, the most straightforward model describing jumps of protons between crystallographic sites is the so-called Chudley–Elliot model.[27] Under the assumption of an isotropic diffusion because of the three-dimensional arrangement of the water molecules, the width $\Delta_{TD}(Q)$ is then given by the following equation:

$$\Delta_{TD}(Q) = \frac{1}{\langle \tau_{TD} \rangle}\left[1 - \frac{\sin(Q\cdot\langle d_{TD}\rangle)}{Q\cdot\langle d_{TD}\rangle}\right] \quad (10)$$

where $\langle \tau_{TD} \rangle$ is the mean residence time of the proton on each site between two consecutive instantaneous jumps and $\langle d_{TD} \rangle$ is the mean jump distance. In the low-Q limit (i.e., over long translational distances), the width $\Delta_{TD}(Q)$ tends toward Fick's law, for which D_{TD} is related to the mean jump distance and the mean residence time by

dx.doi.org/10.1021/jp504128m | J. Phys. Chem. B XXXX, XXX, XXX–XXX

$$D_{TD} = \frac{\langle d_{TD}\rangle^2}{6\langle \tau_{TD}\rangle} \quad (11)$$

The jump-diffusion model has been fitted to the Q dependence of the HWHMs measured by means of QENS. In the fitting procedure, the free parameters were the mean jump distance and the mean residence time. As shown in Figure 6, an excellent agreement is obtained between this model and the experimental HWHMs. The fitted mean residence times (given in Table 1) combined with the mean jump distance lead to the diffusion coefficients D_{TD} in good agreement with those determined by means of ^{1}H PFG-NMR, as shown in Figure 3. The fitted mean jump distance is temperature independent with a value of $\langle d_{TD}\rangle$ = 2.79 ± 0.17 Å. This distance matches with the averaged oxygen−oxygen distance between water molecules determined as 2.8 Å by means of X-ray diffraction in strong acid clathrate hydrates.[12,14,22] Finally, using eqs 10 and 11, the HWHMs $\Delta_{TD}(Q)$ calculated from the ^{1}H PFG-NMR diffusion coefficients by using the mean jump distance $\langle d_{TD}\rangle$ = 2.79 Å are reported in Figure 6. Again, these ^{1}H PFG-NMR-derived HWHMs are in good agreement with the HR-QENS experimental data. Finally, the temperature dependence of the diffusion coefficients (measured by means of PFG-NMR and QENS on $HPF_6{\cdot}7.67H_2O$ and $HPF_6{\cdot}6.5H_2O$ clathrate hydrates) follows an Arrhenius law characterized by a weak activation energy of 0.19 ± 0.04 eV.

4. CONCLUDING REMARKS

Long-range proton diffusion of the $HPF_6{\cdot}7.67H_2O$ and $HPF_6{\cdot}6.5H_2O$ clathrate hydrates has been analyzed by combining ^{1}H PFG-NMR and QENS experiments at temperatures ranging from 90 K to room temperature. The thermal dependence of both sets of data suggests that the HPF_6 clathrate hydrate undergoes a phase transition at ca. 230 K characterized by a hysteresis in the diffusion process. This transition corresponds to the structural transition between the type SI structure below ca. 230 K and the type SVII structure above ca. 230 K.[13] Moreover, the QENS and NMR data exhibit also a signal characteristic of immobile proton on a time scale typically of the order of the nanosecond in the SVII phase. Such results are representative of a reconstructive phase transition between the type SI clathrate hydrate in the low temperature phase and a mixture of type SVII clathrate hydrate and of additional water molecules forming ice in the high temperature phase. In the SI phase of the HPF_6 clathrate hydrate, no long-range proton diffusion is observed either by means of ^{1}H PFG-NMR or by means of QENS. In other words, the diffusion coefficient of protons is smaller than ca. 10^{-7} cm^2/s. Such a result is in agreement with the proton diffusion coefficient measured in the perchloric acid clathrate hydrate, also of type SI: 3.5×10^{-8} cm$^2{\cdot}$s^{-1} at 220 K.[24] In the SVII phase of the HPF_6 clathrate hydrate (i.e., between ca. 230 K and room temperature), the long-range proton diffusion has been analyzed, giving a diffusion coefficient of 3.85×10^{-6} cm$^2{\cdot}$s^{-1} at 275 K with an activation energy of 0.19 ± 0.04 eV. To our knowledge, such diffusion coefficients appear to be one of the most important measured in the case of ionic clathrate hydrate. While the "macroscopic" behavior of the proton diffusion is well determined by means of ^{1}H PFG-NMR, the QENS experiments allow accessing the microscopic mechanism of this diffusion. Results from both techniques are in excellent agreement and lead to the representation of the long-range proton diffusion microscopic mechanism with the help of the Chudley−Elliot jump diffusion model characterized by a 2.79 ± 0.17 Å jump distance. Such a distance corresponds to the oxygen−oxygen distance in the structure SVII aqueous framework.[14,22] The superconductivity of acid clathrate hydrate, attributed to proton diffusion along the clathrate aqueous framework, results from a series of proton jumps from oxygen to another, which is in good agreement with the Grotthuss mechanism. According to this mechanism, several localized dynamical processes (e.g., water molecule reorientations) are involved and occur on a broad time scale, as it has been shown in the case of the perchloric acid clathrate hydrate.[25] In the present study, the mean time associated with these localized dynamical processes has been measured as 2.5 ± 1.2 ps at 255 K with an activation energy of 0.24 ± 0.04 eV. The localized diffusive motions of the proton surrounding the oxygen sites thus occur more frequently than the proton jump between oxygen sites over a long range (see Table 1). However, despite this time scale difference, the energy barrier associated with the long-range diffusion (0.19 ± 0.04 eV) is slightly smaller than the energy barrier associated with localized diffusive motions (0.24 ± 0.04 eV). In other words, the limiting step for the proton conductivity occurs on a local spatial scale: such an experimental observation is in agreement with a theoretical approach on acidic solutions (e.g., phosphoric acid[28]) or with an experimental approach on other acidic clathrate hydrates (e.g., perchloric acid clathrate hydrate[24,25]), suggesting that the acidic proton surrounding plays a key role in the long-range proton diffusion.

The proton diffusion results obtained in the present study may be compared with conductivity measurements performed on the $HPF_6{\cdot}7.67H_2O$ sample for the structure SI[11] and on the $HPF_6{\cdot}6H_2O$ sample for the structure SVII.[13] As seen in Figure 3, the thermal behavior of the conductivity matches the one of the measured diffusion coefficient, as expected with the Nernst−Einstein relationship. Nevertheless, a slight difference is observed in the SVII phase. The conductivity measurement leads to an activation energy of 0.10 eV in the $HPF_6{\cdot}6H_2O$ clathrate hydrates,[13] while an activation energy of 0.19 ± 0.04 eV is found in the present study of the long-range proton diffusion. The conductivity measurement[13] made as a function of water content shows that the best electrochemical properties are obtained for the $HPF_6{\cdot}6H_2O$ clathrate hydrates corresponding to the "ideal" type SVII clathrate structure (with all cages filled) and that increasing the water content leads to a decrease of the protonic conductivity. The present study has been performed on the $HPF_6{\cdot}7.67H_2O$ and $HPF_6{\cdot}6.5H_2O$ clathrate hydrates at temperatures corresponding to a mixture of phases, i.e., the structure SVII clathrate hydrate phase and the ice phase. The higher activation energy found in the present analysis shows that the additional water molecules existing in the SVII structure (forming the ice phase) act as a "structural defect" barrier for the proton diffusivity responsible for the conductivity. Such an interpretation is in agreement with the general description of proton motion in ice; i.e., the proton diffusion occurs on a faster time scale on the surface than in the bulk of ice particle.[29] Although the ice protons are not immobile, as suggested in "soft-landing" of protons on the ice surface,[30] the characteristic diffusion time of ice protons is typically of the order of microseconds.[29] In the present study, the protons participating to the ice "structural defects" are dynamically frozen on the time scale of the PFG-NMR and QENS experiments. The "structural defect" barrier effect is thus associated with proton diffusion in the ice phase that is

dx.doi.org/10.1021/jp504128m | J. Phys. Chem. B XXXX, XXX, XXX−XXX

occurring on a time scale significantly longer than the one of proton diffusion in the SVII clathrate hydrate phase (of the order of 0.1 ns).

AUTHOR INFORMATION

Corresponding Author

*E-mail: a.desmedt@ism.u-bordeaux1.fr. Phone: ++33 5 4000 2937. Fax: ++33 5 4000 6994.

Present Address

#Institut Charles Sadron, CNRS-Université de Strasbourg, 23 rue du Loess, B.P. 84047, 67034 Strasbourg Cedex 2, France.

Notes

The authors declare no competing financial interest.

ACKNOWLEDGMENTS

A.D. wishes to thank the Institut Laue Langevin neutron facilities in Grenoble (France) and the staff members for the beam time allocation, for the support and for the cofunding with the CNRS of Laura Bedouret's Ph.D. This paper falls in the frame of the project ANR 2011-JS08-002-01, funded by the French "Agence Nationale de la Recherche".

REFERENCES

(1) Sloan, E. D.; Koh, C. A. *Clathrate Hydrates of Natural Gases*, 3rd ed.; Taylor & Francis-CRC Press: Boca Raton, FL, 2008.

(2) Jeffrey, G. A. Hydrate Inclusion Compounds. In *Comprehensive Supramolecular Chemistry*; Atwood, J. L., Davies, J. E. D., Mac-Nicol, D. D., Vögtle, F., Eds; Pergamon: Oxford, U.K., 1996; Vol. *6*, p 757.

(3) Desmedt, A.; Bedouret, L.; Pefoute, E.; Pouvreau, M.; Say-Liang-Fat, S.; Alvarez, M. Energy Landscape of Clathrates Hydrates. *Eur. Phys. J.: Spec. Top.* **2012**, *213*, 103−127.

(4) Koh, C. A.; Sloan, E. D. Natural Gas Hydrates: Recent Advances and Challenges in Energy and Environmental Applications. *AIChE J.* **2007**, *53*, 1636−1643.

(5) Sloan, E. D. Fundamental principles and applications of natural gas hydrates. *Nature* **2003**, *426*, 353−363.

(6) Shin, K.; Cha, J.; Seo, Y.; Lee, H. Physicochemical Properties of Ionic Clathrate Hydrates. *Chem.—Asian J.* **2010**, *5*, 22−34.

(7) Borkowska, Z.; Tymosiak, A.; Opallo, M. Conductivity of Stoichiometric $(CH_3)_4NOH$ Clathrate Hydrates. *J. Electroanal. Chem.* **1996**, *406*, 109−117.

(8) Opallo, M.; Tymosiak, A.; Borkowska, Z. Conductivity of Tetramethylammonium Fluoride Tetrahydrate. *J. Electroanal. Chem.* **1995**, *387*, 47−52.

(9) Cappadonia, M.; Kornyshev, A. A.; Krause, S.; Kuznetsov, A. M.; Stimming, U. Low Temperature Proton Transport in Clathrates. *J. Chem. Phys.* **1994**, *101*, 7672−7682.

(10) Huang, T.-H.; Davis, R. A.; Frese, U.; Stimming, U. Proton Mobility in Liquid and Frozen $HClO_4 \bullet 5.5H_2O$: NMR and Conductivity Measurements. *J. Phys. Chem.* **1988**, *92*, 6874−6876.

(11) Aschrafi-Mahabadi, S.; Cappadonia, M.; Stimming, U. Proton Transport in Solid Electrolytes with Clathrate Structure. *Solid State Ionics* **1994**, *70/71*, 311−315.

(12) Mootz, D.; Oellers, E. J.; Wiebcke, M. First Examples of Type I Clathrate Hydrates of Strong Acids: Polyhydrates of Hexafluorophosphoric, Tetrafluoroboric, and Perchloric acid. *J. Am. Chem. Soc.* **1987**, *109*, 1200−1202.

(13) Cha, J.; Shin, K.; Choi, S.; Lee, S.; Lee, H. Maximized Proton Conductivity of the HPF_6 Clathrate Hydrate by Structural Transformation. *J. Phys. Chem. C* **2008**, *112*, 13332−13335.

(14) Bode, V.; Teufer, G. Die Kristallstruktur der Hexafluorophosphorsäure. *Acta Crystallogr.* **1955**, *8*, 611−614.

(15) Altieri, S.; Hinton, D. P.; Byrd, R. A. Association of Biomolecular Systems via Pulsed Field Gradient NMR Self-Diffusion Measurements. *J. Am. Chem. Soc.* **1995**, *117*, 7566−7567.

(16) Stejskal, E. O.; Tanner, J. E. Spin Diffusion Measurements: Spin Echoes in the Presence of a Time-Dependent Field Gradient. *J. Chem. Phys.* **1965**, *42*, 288−292.

(17) Frick, B.; Gonzalez, M. Five Years Operation of the Second Generation Backscattering Spectrometer IN16 - a Retrospective, Recent Developments and Plans. *Physica B* **2001**, *301*, 8−19.

(18) Ollivier, J.; Mutka, H. IN5 Cold Neutron Time-of-Flight Spectrometer, Prepared to Tackle Single Crystal Spectroscopy. *J. Phys. Soc. Jpn.* **2011**, *80*, SB003-1−SB003-6.

(19) Anderson, I.; Nelson, R. *Institut Laue-Langevin Technical Report 85AN8T*, 1985.

(20) Contact A. Desmedt for further details.

(21) Bée, M. *Quasielastic Neutron Scattering: Principles and Applications in Solid State Chemistry, Biology and Materials Science*; Adam Hilger: Bristol and Philadelphia, PA, 1988.

(22) Wiebke, M.; Mootz, D. Die isotypen Phasen $HEF_6 \cdot 5H_2O \cdot HF$ (E = P, As, Sb): Neubestimmung der Strukturen an Einkristallen. *Z. Kristallogr.* **1986**, *177*, 291−299.

(23) Roussel, F.; Judeinstein, P. Diffusion Processes in Homogeneous and Phase-Separated Binary Fluid Mixtures. *Soft Matter* **2008**, *4*, 888−892.

(24) Desmedt, A.; Stallmach, F.; Lechner, R. E.; Cavagnat, D.; Lassègues, J. C.; Guillaume, F.; Grondin, J.; Gonzalez, M. A. *J.*, Proton Dynamics in the Perchloric Acid Clathrate Hydrate $HClO_4 \bullet 5.5H_2O$. *Chem. Phys.* **2004**, *121*, 11916−11926.

(25) Desmedt, A.; Lechner, R. E.; Lassègues, J. C.; Guillaume, F.; Cavagnat, D.; Grondin, J. Hydronium Dynamics in the Perchloric Acid Clathrate Hydrate. *Solid State Ionics* **2013**, *252*, 19−25.

(26) Desmedt, A.; Soetens, J. C.; Prager, M.; Russina, M.; Ollivier, J. Diffusive Motions of Molecular Hydrogen Confined in THF Clathrate Hydrate. *J. Phys. Chem. C* **2011**, *115* (26), 12823−16829.

(27) Chudley, C. T.; Elliott, R. J. Neutron Scattering from a Liquid on a Jump Diffusion Model. *Proc. Phys. Soc., London* **1961**, *77*, 353−361.

(28) Vilciauskas, L.; Tuckerman, M. E.; Bester, G.; Paddison, S. J.; Kreuer, K. D. The Mechanism of Proton Conduction in Phosphoric Acid. *Nat. Chem.* **2012**, *4*, 461−466.

(29) Devlin, J. P. Relating the Current Science of Ion-Defect Behavior in Ice to a Plausible Mechanism for Directional Charge Transfer during Ice Particle Collisions. *Phys. Chem. Chem. Phys.* **2011**, *13*, 19707−19713.

(30) Cowin, J. P.; Tsekouras, A. A.; Iedema, M. J.; Wu, K.; Ellison, G. B. Immobility of Protons in Ice from 30 to 190 K. *Nature* **1999**, *398*, 405−407.